



Research paper

Extraction of plasticity parameters from a single test using a spherical indenter and FEM modelling



J. Dean, T.W. Clyne*

Department of Materials Science & Metallurgy, Cambridge University, 27 Charles Babbage Road, Cambridge CB3 0FS, UK

ARTICLE INFO

Article history:

Received 22 August 2016

Revised 29 November 2016

Available online 9 December 2016

Keywords:

Indentation

Finite element analysis

Plasticity

ABSTRACT

A methodology is presented for obtaining plasticity characteristics of bulk metallic materials from single run indentation data. It involves repeated FEM modelling, with the predicted outcome (load-displacement plot) being systematically compared with experiment. The “correct” property values are found by searching for the combination giving the maximum value for a “goodness of fit” parameter (g) measuring the agreement between experimental and predicted outcomes (ranging from 0 for no agreement to 1 for perfect agreement). A matrix of property values are used as input data for the FEM model. The key issue is that of promoting convergence on the “correct” parameter combination. It is becoming accepted that use of more than one indenter shape will assist in this operation and the paper includes an exploration of this issue. It is emphasized that the strain field beneath an indenter affects the relationship between stress-strain curve and load-displacement plot, so use of shapes that create different strain fields adds extra degrees of freedom that facilitate convergence. However, there are various problems associated with use of indenters having “sharp” points or edges, and a spherical shape is much preferred. It is highlighted here that, provided the indenter shape is not self-similar (so that the nature of the strain field changes with increasing penetration depth), analogous benefits to those arising from multiple shapes can be obtained by carrying out “ g -screening” operations on multiple sections of a single load-displacement plot. This is an entirely novel approach that offers considerable promise for the tractable characterization of plasticity via a single indentation run with a spherical indenter. It has been employed in the present work to obtain values of three plasticity parameters from such a run for an extruded copper sample. In fact, the stress-strain curve for this material is not one that conforms closely to a simple analytical formulation, imposing a limit on the fidelity of the inferred stress-strain curve, but it is nevertheless shown that the proposed procedure is viable and potentially very accurate.

© 2016 The Authors. Published by Elsevier Ltd.

This is an open access article under the CC BY license (<http://creativecommons.org/licenses/by/4.0/>).

1. Introduction

There has been increasing focus over the past decade or two on the important objective of obtaining (engineering or true) stress-strain curves (beyond the elastic limit) from instrumented indentation data (mainly load-displacement plots). Since these stress-strain curves are regarded as prime indicators of the plasticity characteristics of a material, and indentation is a much more versatile and convenient procedure than conventional uniaxial testing, this quest has a strong motivation. The approaches used fall into two main categories. Most studies have sought to identify analytical formulations that can be applied to the experimental data. This has obvious attractions, since such a formulation, even if involving relatively complex expressions and algorithms, would allow rapid extraction of the stress-strain curves via a well-defined path. Un-

fortunately, the stress and strain fields beneath an indenter, even one with a simple shape such as a sphere, are complex and change with penetration depth, making it difficult to identify realistic analytical relationships.

Of course, for a material with a given (uniaxial) stress-strain curve, assumed to be applicable to deviatoric (von Mises) components of stress and strain for multi-axial situations, the load-displacement plot during indentation can be predicted (using FEM), for any given indenter shape. However, the inverse problem of inferring the stress-strain relationship from such a load-displacement plot is much more challenging, with considerable scope for ambiguity (different stress-strain relationships giving effectively the same load-displacement plot). In fact, this problem is the main obstacle for the second category of approach (Dao et al., 2001; Bolzon et al., 2004; Bouzakis and Michailidis, 2004; Bouzakis and Michailidis, 2006; Pelletier, 2006; Guelorget et al., 2007; Heinrich et al., 2009; Dean et al., 2010; Bobzin et al., 2013; Patel and Kalidindi, 2016), which is simply to carry out iterative FEM mod-

* Corresponding author.

E-mail address: twc10@cam.ac.uk (T.W. Clyne).

eling of the indentation process using various trial stress-strain curves (characterized via a set of parameter values) and converge on the set giving optimum agreement with the experimental load-displacement plot. This is at least a transparent and rigorous procedure, although its wide implementation is inhibited by the need to carry out FEM modeling runs that are specific to each individual case, as well as by the “uniqueness” problem.

For both types of approach, it has been recognized (Futakawa et al., 2001; Bucaille et al., 2003; Capehart and Cheng, 2003; Chollacooop et al., 2003; Cheng and Cheng, 2004; Ma et al., 2012) that there may be advantages in obtaining more comprehensive sets of experimental data. It is well understood that the stress and strain fields beneath an indenter are scale-independent. For example, the fields created by penetration of a sphere to a depth corresponding to, say, 10% of its radius are identical for radii of, say, 10 μm and 10 mm. (The absolute value of the load at this point will be 10^6 greater for the latter case, while the penetration will be 10^3 greater, but the information being provided about the stress-strain response of the material is the same, provided the volume being interrogated is in both cases large enough to be representative of the bulk response.)

However, if further (different) shapes are used, for example by testing with a cone, in addition to a sphere, then the different relationship between the stress and strain fields in the sample and the measured load-penetration plot introduces extra degrees of freedom and reduces the likelihood of ambiguity, facilitating convergence on the correct set of plasticity parameters and raising the level of confidence in their reliability. In fact, a similar type of improvement can also be obtained by expanding the range of experimental outcomes being considered - for example, encompassing the residual indent shape, as well as the load-displacement plot - although this is likely to make the whole process more cumbersome, both experimentally and in terms of the convergence algorithm.

For any approach involving realistic representation of the stress and strain fields, the relationship between them - ie the material plasticity response - must be characterized via a set of parameter values: in fact, several formulations are in use, but the following expression is most commonly employed

$$\sigma = \sigma_Y + K \varepsilon_p^n \quad (1)$$

where σ is the (von Mises) applied stress, σ_Y is its value at yield, ε_p is the plastic (von Mises) strain, K is the work hardening coefficient and n is the work hardening exponent, so that there are 3 parameter values in the general case. If $K=0$, then there is no work hardening (“perfectly plastic”) and the behaviour is characterised by a single parameter value (σ_Y). If K is non-zero and n has a value of 1, then linear work hardening is exhibited and the behaviour is characterised by two parameter values.

A large number of schemes have been proposed (Cheng and Cheng, 1999; Giannakopoulos and Suresh, 1999; Dao et al., 2001; Herbert et al., 2001; Cheng and Cheng, 2004; Alkorta et al., 2005; Herbert et al., 2006; Xu and Chen, 2010; Hausild et al., 2012; Fu et al., 2015) for inferring such plasticity parameters from indentation data, many based on some sort of minimization of the discrepancy between the values of dimensionless parameters, so as to obtain analytical functions that relate indentation data to elasto-plastic properties. These dimensionless parameters are usually functions of E , σ_Y , K and n , although in some cases they include parameters such as the curvature of the load-displacement plot, the contact stiffness, the ratio between residual penetration and maximum indentation depths and the ratio of plastic work to total work. There are also schemes for converting experimental load-displacement plots to stress-strain curves by identifying “effective” values of both stress and strain at a given penetration

depth. Such formulations often include various kinds of “correction” or “calibration” factors for specific classes of alloy and in general it’s clear that they are far from being universally applicable or reliable. Furthermore, the lack of rigour and transparency about the underlying assumptions means that, even if values can be obtained, there are no real grounds for assessing their accuracy or reliability.

The alternative approach of simply carrying out FEM modelling of the actual indentation process(es) concerned, using trial material properties, and then to iteratively alter these properties until optimal agreement is obtained between predicted and observed experimental outcomes, is now being explored more systematically. Dean et al. (2010) estimated that, typically, the yield stress, σ_Y , could be determined to a precision of about $\pm 10\%$, and the linear work-hardening rate, K , to about $\pm 25\%$. Their method involved iterative variations in the parameter values in a linear work-hardening relationship (ie $n=1$ in Eq. (1)) until optimum agreement was obtained between predicted and measured load-displacement data (in a testing regime in which creep effects could be neglected). The iteration was carried out “manually” and there was no systematic assessment of expected error levels (apart from comparing inferred values with those obtained by conventional testing) or of the uniqueness of solutions. Nevertheless, the results do provide some confirmation that the methodology is basically sound. It’s unsurprising that the precision was lower for K , compared with σ_Y , although this is expected to depend on the plastic strain levels induced during the test.

A potentially useful (dimensionless) parameter in this context is W , defined as the work hardening contribution to the stress, at a given level of plastic strain, relative to the yield stress.

$$W = \frac{K \varepsilon_p^n}{\sigma_Y} \quad (2)$$

For uniaxial loading up to a certain strain level, this would be simple to evaluate. With an inhomogeneous strain field, such as that during indentation, it would be possible to use the maximum level of strain in Eq. (2), although a more logical approach in assessing the influence of work hardening on the outcome would be to use a strain level representing some sort of volume-average, weighted by the proportion of the total amount of plastic work that had been done in the volume elements concerned as indentation proceeds up to a given displacement.

Of course, the main drawback of this “simple” inverse iterative FEM procedure is that it requires the user to carry out dedicated FE modelling for a large number of combinations of the parameter values. This is in practice a major obstacle to widespread use, particularly if the iteration process is poorly-defined. However, if the key features of such iteration procedures can be fully understood, then there will clearly be scope for automation of the convergence process, perhaps to such an extent that the user need not become involved at all with actual FE modelling. Such an automated procedure will clearly need to involve evaluation of a suitable “goodness of fit” parameter, characterizing the level of agreement between experimental and predicted outcomes (such as load-displacement plots). One definition was suggested by Bolzon et al. (2004), who noted that the accuracy of inferred values could be improved if residual indent shapes were taken into account, as well as load-displacement data.

The main requirement now, in order for procedures (and dedicated software packages) to become widely accepted and employed, is clear identification of the factors that affect sensitivities and efficient convergence on “correct” solutions for inferred properties, and selection/testing of an optimized algorithm. This is the focus of the present paper.

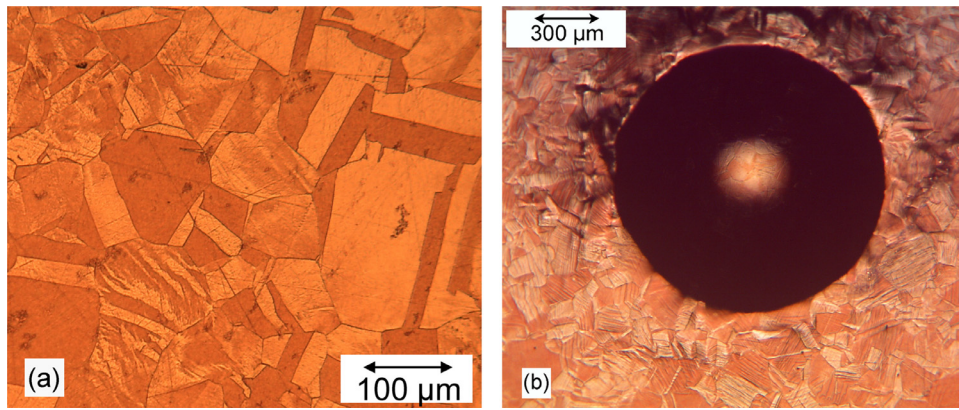


Fig. 1. Optical micrographs of extruded copper (a) as-polished/etched and (b) after indentation with a sphere of diameter 3 mm, to a depth of about 100 μm.

2. Experimental procedures

2.1. Materials and microstructures

An extruded (25 mm diameter) copper bar, in the as-received state, was used in this study. Both conventional compression testing and instrumented indentation were carried out along the extrusion axis. It can be seen in Fig. 1(a) that the grain size (in transverse section) was of the order of 100 μm. Such (relatively coarse) grain structures, which are far from uncommon, do present challenges in terms of using indentation to obtain (bulk) properties, since it's clear that these can only be obtained by mechanically interrogating a representative (multi-grain) volume. The indent in Fig. 1(b), which was created using a large diameter (3 mm) sphere, clearly does this. This issue is addressed in Section 3.3.

2.2. Uniaxial compression testing

In order to obtain the “correct” plasticity parameter values for this material, samples were subjected to uniaxial compression testing between rigid (hardened steel) platens. Cylindrical specimens (5 mm height, 5 mm diameter) were tested at room temperature (20 °C ± 2 °C), using MoS₂ lubricant to minimize barreling. Displacements were measured using a Keyence scanning laser system (and checked with a Linear Variable Displacement Transducer). Both of these systems have a resolution of ~1 μm, and gave very close agreement. Testing was carried out under displacement control (at a rate of 25 μm s⁻¹), using an Instron 5562 screw-driven testing machine, with a load cell having a capacity of 30 kN.

Tests were carried out up to displacements of about 500 μm (10% plastic strain), so that each test took about 20 s to complete. It was confirmed that barreling was negligible over this strain range. In order to check on the possible significance of creep, the displacement was held at 500 μm for a period of 60 s. The load drop over this period was found to be about 50 N (ie a fall of < 1%). This is considered to be negligible in the context of the testing being undertaken (both compression and indentation).

Several repeat tests were carried out. Both stress and strain levels were converted from nominal to true values, using the standard expressions:

$$\sigma_T = \sigma_N (1 + \varepsilon_N), \quad \varepsilon_T = \ln(1 + \varepsilon_N) \quad (3)$$

with the strains in this case being negative (compressive), so that the true stress is lower than the nominal value. The data for a typical run are shown in Fig. 2, plotted as both nominal and true values. The variation between tests was in general very small (< 1%). It can be seen that, as a true stress – true strain relationship, this material exhibits some work hardening, although it's relatively

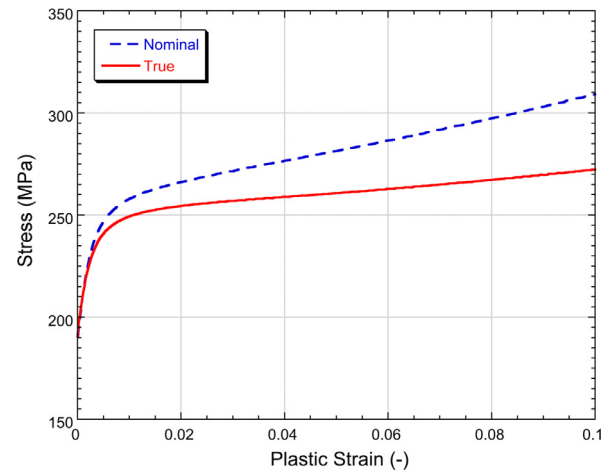


Fig. 2. A typical stress-strain plot from compression testing of a copper sample, plotted as both nominal and true values.

weak - the extrusion process probably left a fairly high level of residual cold work - so that the sensitivity of the indentation response to the work hardening is expected to be relatively low. For example, the value of the ratio W (Eq. (2)) is about 20%, for a plastic strain of 10%. It is also fairly clear from the plot in Fig. 2 that the stress-strain response cannot be captured to very high accuracy by an expression with the form of Eq. (1), since there is a transition from a relatively low value of n at low strains to a more linear plot (n close to 1) at higher strains. This material therefore presents a challenge in terms of accurate evaluation of the work hardening behaviour.

2.3. Instrumented indentation

The loading and strain measurement set-up described above was also used for the indentation testing, this time under load control. A single indenter was used - a sphere of radius 2 mm, made of hardened steel. The load was taken to about 1 kN, corresponding to a displacement of about 100 μm and an impression diameter of just over 1200 μm - see Fig. 1(b) for a similar case. A representative load-displacement plot is shown in Fig. 3.

3. Background to algorithm development

3.1. Goodness of fit Parameter, g

Central to this methodology is the definition of a “goodness of fit” parameter, g , characterizing the level of agreement between

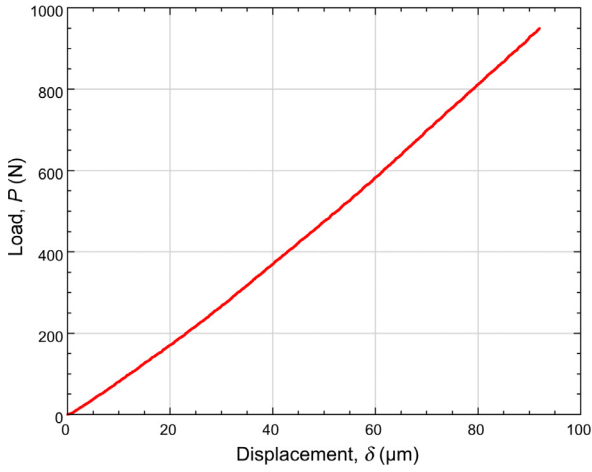


Fig. 3. A typical load-displacement plot obtained during indentation testing of a copper sample, using a spherical indenter of diameter 4 mm.

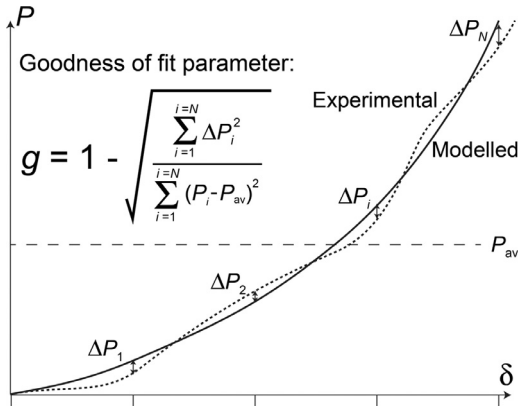


Fig. 4. Schematic of an experimental load-displacement plot, with a modeled prediction superimposed, and the definition of the goodness-of-fit parameter, g .

predicted and measured outcomes. The definition employed (for load-displacement plots) in the current work is:

$$g = 1 - \frac{\sqrt{\sum_{i=1}^N \Delta P_i^2}}{\sqrt{\sum_{i=1}^N (P_i - P_{av})^2}} \quad (4)$$

with the meanings of the parameter values being illustrated in Fig. 4. Comparisons are made between experimental and predicted values of load (P) at a set of N values of the displacement, δ . This is done at selected displacement intervals and, in the present work, the value of N was typically about 100. It is clear from the form of Eq. (4) that perfect agreement between the two sets of data ($\Delta P_i = 0$ for all i values) gives a value for g of 1, while no agreement (ie predictions random about the average value) leads to a value of 0.

It should be emphasized that alternative definitions for a goodness-of-fit parameter can be devised. For example, incremental scanning could be carried out on the y -axis (P values), instead of, or in addition to, that along the x -axis. Furthermore, definitions are possible for which perfect agreement corresponds to $g = 0$, with the sign of the g value indicating whether, on average, predicted loads are above or below the reference (experimental) values. However, the definition used here serves to illustrate the main features of g -scanning operations.

3.2. FEM modelling

Axi-symmetric FEM models were built using COMSOL multi-physics. Both indenters and samples were modelled as deformable bodies and meshed with second order quadrilateral and/or triangular elements. While the indenter is expected to remain elastic throughout, it can be important in high precision work of this nature not to treat it as a rigid body: not only is it possible for its elastic deformation to make a significant contribution to the overall displacement, but its lateral Poisson expansion could affect the outcome, particularly if attention is being focused on the shape of the residual impression. Such simulation of the indenter deformation was particularly important in the present work, based on using steel indenters (with relatively low stiffness and relatively high Poisson ratio), but in fact it should be carried out in all cases in which high precision is required. Of course, such modeling also allows a check to be made on whether there is any danger of the indenter being plastically deformed.

Meshes were, of course, refined in regions of the sample close to the indenter. Sensitivity analyses confirmed that the meshes employed were sufficiently fine to achieve convergence, numerical stability and mesh-independent results. The situation regarding the extent of the sample being represented in the simulation should also be noted. The lateral extent is of little significance, provided it extends well beyond the region of plastic deformation and provides representative constraint. In the loading direction, however, there is the issue of whether the contribution to the measured deflection caused by elastic deformation of the sample is being fully captured. It is conventional to locate the sample on a flat, rigid surface that remains fixed. The displacement during indentation is then the change in separation between that level and another flat, rigid surface, to which the indenter is attached. The thickness of the sample in the simulation must be sufficient to capture all of the contribution to the displacement from its elastic deformation (as well as its plastic deformation). In practice, however, the stress, and hence the elastic strain, in the sample drop off with distance from the indenter and, at least in most cases, will become negligible well above the bottom of the sample. In the present work, the sample thickness in the simulations was at least 5 times the depth to which plastic deformation extended during the test and it was confirmed that this was sufficient to ensure that the contribution to the overall displacement from its elastic deformation was accurately captured.

The simulation runs were carried out under displacement control, with the output being the predicted load at a series of (~ 100) specified displacement values ($1 \mu\text{m}$ intervals) over the range concerned. The residual indent shape, and the surrounding fields of residual stress and plastic strain, were also predicted in each case. All material properties were assumed to be isotropic. For the illustrative runs (Sections 3.4 and 4), the Young's moduli of indenter and sample were respectively taken to be 210 GPa (steel) and 120 GPa (copper), while the Poisson ratios were both taken to be 0.3. The same values were used for the comparisons with experimental data obtained using the copper (Section 5).

The meshes employed are shown in Fig. 5, corresponding to the three indenter shapes used in these simulations (Section 4). Also shown in the figure are the plastic strain fields for three different penetrations, for a reference case of $\sigma_y = 300 \text{ MPa}$, $K = 1000 \text{ MPa}$ and $n = 1$. It's important to appreciate that these strain fields are independent of scale - see Section 3.3 below. It can be seen in this figure that the strain fields are substantially different for these three cases, both in terms of the distribution of the strains and their magnitudes. These differences in strain distribution are relevant to the algorithm for extraction of the plasticity parameters - see Section 4. It can also be seen that, for the only self-similar shape (the cone), the nature of the strain field is independent of

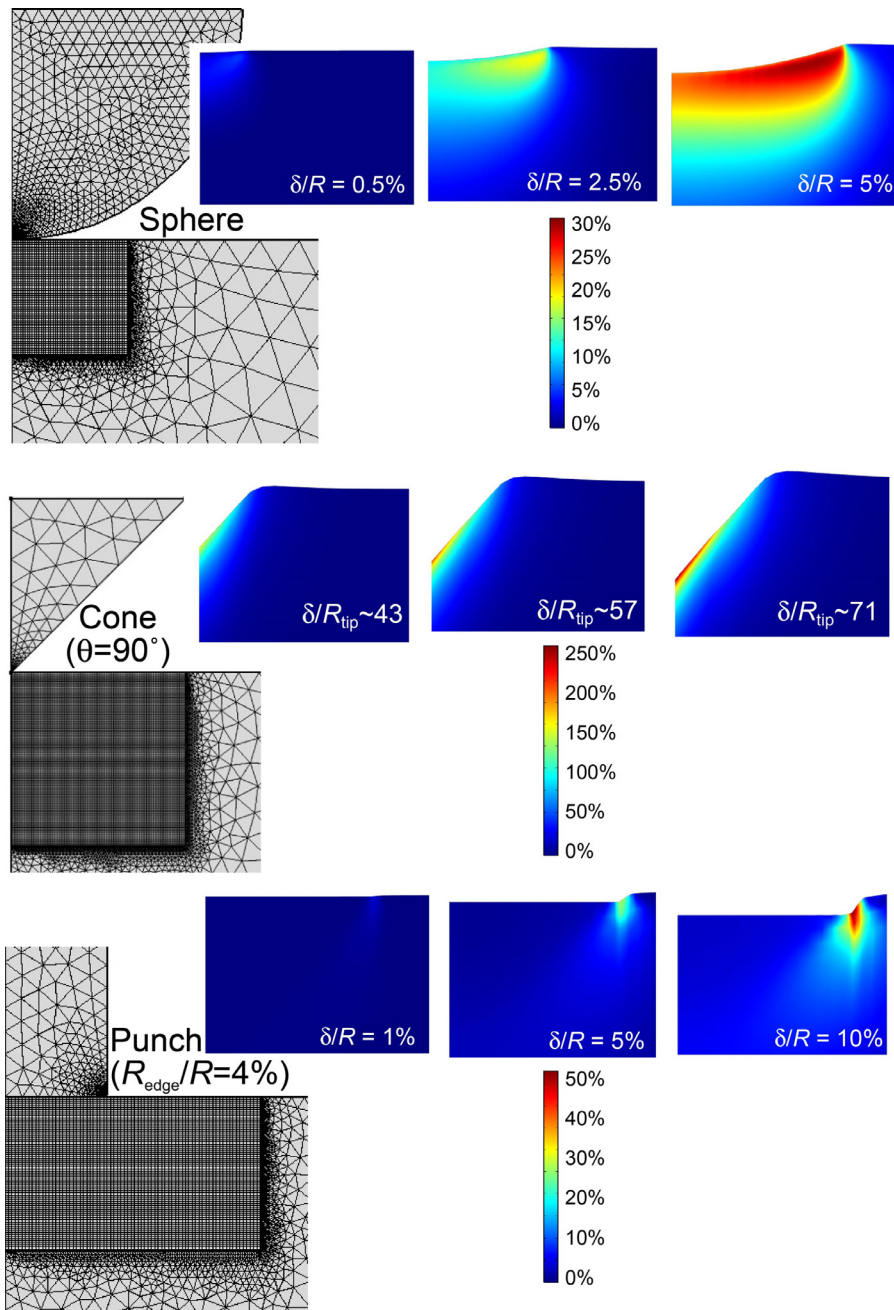


Fig. 5. FEM meshes used for the sphere, cone and cylindrical punch, with corresponding fields of (von Mises) plastic strain after three different extents of penetration.

penetration¹ (although the magnitude of the strains does increase with penetration), whereas for the other two (non-self-similar) shapes, it is not.

3.3. Scale of indentation

Important benefits arise, when the objective is to extract bulk properties, from carrying out the testing on a relatively coarse scale (while retaining the key advantages of being able to test small, flat samples, to carry out point-to-point mapping of properties etc). In particular, the volume being interrogated must have a response that is representative of the bulk. While much recent

indentation research has focused on very fine scales, it is arguably on this “meso” scale (such that indents are large enough for representative material response, but small enough to allow small samples and mapping) that the main potential for increased industrial usage of indentation lies. The minimum indent size for representative response depends on microstructure, but in many cases it will require deformation of an assembly of grains - perhaps at least about a dozen and preferably more. A crude rule of thumb might be that, viewed on the free surface, the indent should straddle at least “several” grains. Of course, the corresponding minimum indent diameter might range from below $1\ \mu\text{m}$ to above $1\ \text{mm}$, but it will certainly be small enough in most cases to offer the attractions outlined above.

In the current case, the grain size is about $100\ \mu\text{m}$ (Fig. 1), so it was ensured that all indent diameters were at least a few

¹ This is the case when the penetration is much greater than the radius at the tip of the cone, as for the simulations shown.

hundred microns - see Fig. 1(b) for a typical indent produced using a sphere. This does require relatively large indenters (\sim mm dimensions) and also large loads (\sim hundreds of N, or even a few kN), which may be beyond the range of some indentation systems (but perhaps below the commonly-used ranges of some conventional mechanical testing systems). However, systems in this “intermediate” load range are in general easier and cheaper to construct and use than either of the other two types of system. Moreover, a relatively coarse scale of indentation minimizes the problems associated with surface roughness, oxide films, contamination etc. Of course, there may still be advantages in locating such systems within a vacuum chamber, facilitating testing at high and low temperatures, and reducing the problems associated with oxidation of sample or indenter.

3.4. Shape of indenter

Regarding the role of indenter shape, axial symmetry has clear attractions, particularly when large numbers of FEM modeling runs will be required. (Of course, the sample may be transversely anisotropic, which would be apparent from the shape of the indent, although in most cases such anisotropy is small.) This still leaves, however, considerable potential for creating different types of strain field, since the shape can vary from a sphere, through various types of cone, to a cylindrical punch.

For (axi-symmetric) indenter shapes other than a sphere, such as a cone, there will be more than one shape parameter (eg cone angle and tip radius), but the same arguments about scale apply. The differences between the plastic strain fields beneath indenters with different shapes are important, since they lead to sample responses that will depend on the plasticity parameters of the material in different ways, and hence are providing different information about them. Strain fields are shown in Fig. 5 under indenters with three different shapes, for three different penetrations in each case. As many workers have highlighted, there are potential advantages in using more than one indenter shape, in terms of convergence on the “correct” set of parameter values, and this is also illustrated below (Section 4).

However, it’s also important to recognize the disadvantages associated with many (non-spherical) shapes. Most such shapes incorporate “sharp” edges or points of some sort. In practice, these regions must have a finite radius and that value may be difficult to establish (and prone to change and shape degradation during service). Furthermore, as can be seen in Fig. 5, the strains in the sample close to these regions (when a suitable tip or edge radius is used in the model) are predicted to become large, even for relatively small penetrations. This makes the load-displacement response sensitive to very high strain regions of the stress-strain curve, where it is in fact unlikely to conform to the plot extrapolated from the lower strain regime (and where, in practical terms, there is probably little interest in the behavior). There is in general no doubt that a sphere is by far the most convenient and theoretically attractive shape to use.

The relationship between the uniaxial stress-strain curve and the indentation load-displacement plot, for a given indenter shape and penetration depth, is clearly of importance. As was mentioned in Section 1 (Eq. (2)), the sensitivity of the indentation outcome to the work hardening characteristics will depend on the value of the parameter W , but there is potential uncertainty about the value of the plastic strain to use in this equation (since the maximum value will in most cases be generated only in a small volume and the behavior in that regime of strain will have little influence on the overall outcome). The plot in Fig. 6 is relevant to this issue. It shows, for a spherical indenter, how the peak strain in the sample increases as the penetration is raised (up to $\delta/R = 5\%$, which is one of the cases shown in Fig. 5). Also shown is the weighted aver-

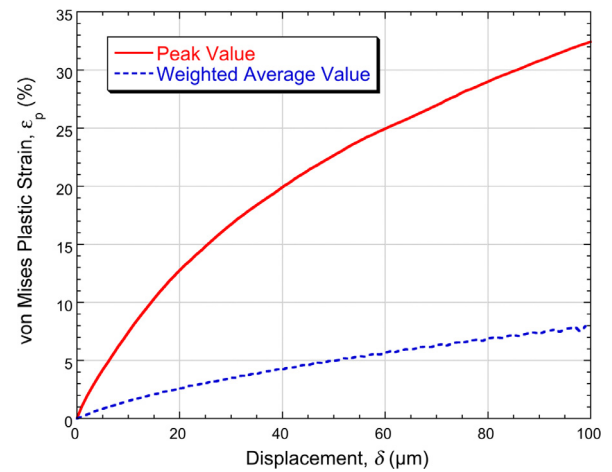


Fig. 6. Predicted value of the peak strain within a sample, as a function of the penetration depth of a spherical indenter of radius 2 mm (up to a value corresponding to $\delta/R = 5\%$). Also shown is the corresponding weighted average plastic strain within the sample.

age strain. The averaging procedure, over all volume elements experiencing plastic strain (up to the penetration depth concerned), involved weighting by the plastic work done at each strain level. It can be taken as some sort of effective strain level to which the response up to the penetration concerned is sensitive. (This plot was produced using $\sigma_Y = 300$ MPa, $K = 1000$ MPa and $n = 1$, but it can be taken as broadly illustrative.) It can be seen that, for example, while penetration to a depth of $100 \mu\text{m}$ creates some large strains ($\sim 30\%$), these are in a small volume (and are only created towards the end of the run), and the overall outcome of such a test is mainly sensitive to the nature of the stress-strain curve in a regime with an average value around 8%.

Finally, the issue of the smoothness of the surfaces of both the indenter and the sample is worthy of attention. Analysis is certainly simplified if frictional effects can be neglected. Most studies of this issue have concluded that the coefficient of friction is usually low during indentation and, even if it’s not, the resultant changes in behavior are relatively small. Nevertheless, there are clear advantages in the surfaces being smooth on the scale of interest. This is often the case, although the problems naturally get worse as the indenter size is reduced. It is in any event worth noting that the early part of a load-displacement plot, where the penetration depth is similar in magnitude to the surface roughness, is unlikely to yield highly accurate or reliable data.

4. Algorithm for extraction of plasticity parameter values

4.1. Perfectly plastic material (no work hardening)

This is, of course, the simplest case, with just one parameter (σ_Y) to evaluate, and hence the treatment is easy to follow. Taking the (“correct”) value to be 300 MPa, and running the FEM model for a sphere, leads to the load-displacement plot shown in Fig. 7(a), which also includes plots for another two σ_Y values (270 and 330 MPa). Comparing these two plots with the “correct” one, and applying Eq. (4), leads to values for g of 0.820 and 0.855. If the 300 MPa plot were an experimental one, then these values of g would characterize the goodness of fit for the 270 and 330 MPa trial values. This operation can, of course, be carried out for a series of trial values. Fig. 7(b) shows the corresponding set of g values, for the three indenter shapes. It naturally has a value of 1 for $\sigma_Y = 300$ MPa, and falls away on either side. With an experimental plot as the “reference case”, g will never reach 1 for any trial value, but Fig. 7(b) gives an indication of the expected sensitivity.

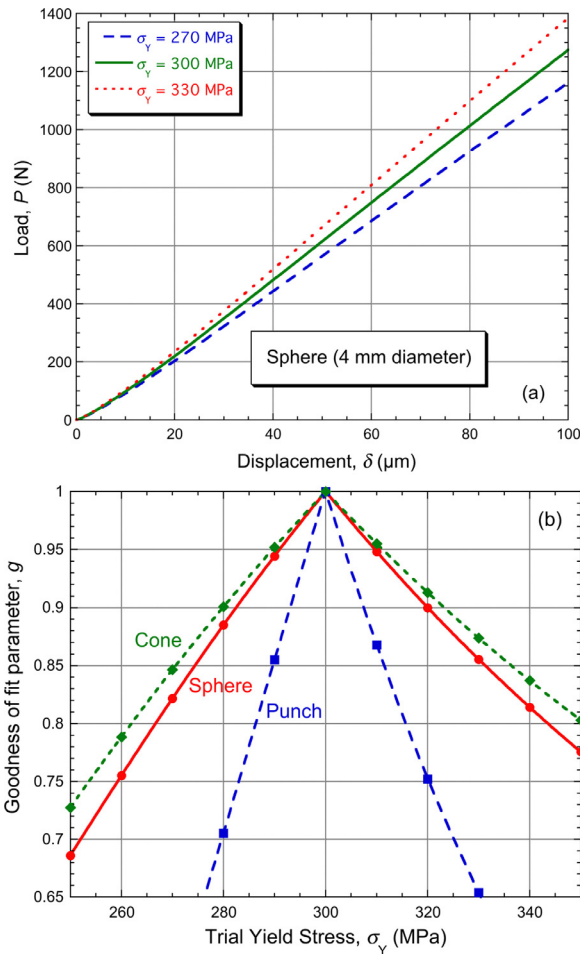


Fig. 7. FEM outcomes for a material exhibiting no work hardening and a “correct” yield stress of 300 MPa: (a) load-displacement plots for a 4 mm diameter sphere, using this value and two others, and (b) plot of g as a function of the trial value, over a range either side of the “correct” one, for three indenter shapes.

It does offer encouragement, in the sense that, in all cases, g falls off quite sharply with relatively small deviations from the “correct” value. It’s also clear that the drop-off is sharpest with the punch and most gradual with the cone. This would not have been easy to predict, although it can be rationalized in terms of the plastic strain fields - for example, the high plastic strains (in a relatively large volume) around the edge of the punch will tend to make the load-displacement plot more sensitive to the yield stress. However, as was noted in Section 3.4, there are problems associated with usage of any indenter having “sharp” (ie very high curvature) regions.

4.2. Linear work hardening material

Following a similar procedure, the (“correct”) value of σ_Y is retained at 300 MPa, in combination now with a linear ($n=1$) work hardening rate, K , of 1000 MPa. Various trial combinations of σ_Y and K are now possible, each leading to a particular value of g by comparing the resultant $P(\delta)$ plot with that for the “correct” combination. The set of g values obtained by running the model with a matrix of such trial combinations is represented in Fig. 8(a)–(c), for sphere, cone and punch. These plots are maps in σ_Y – K space, with each g value having been put into one of 5 ranges.

It can be seen in Fig. 8(a) and (b) that, envisaged as a 3-D contour plot, there are “ridges” (running through the “correct” value pair) of pairs with high g values (>0.97) - these are plotted as

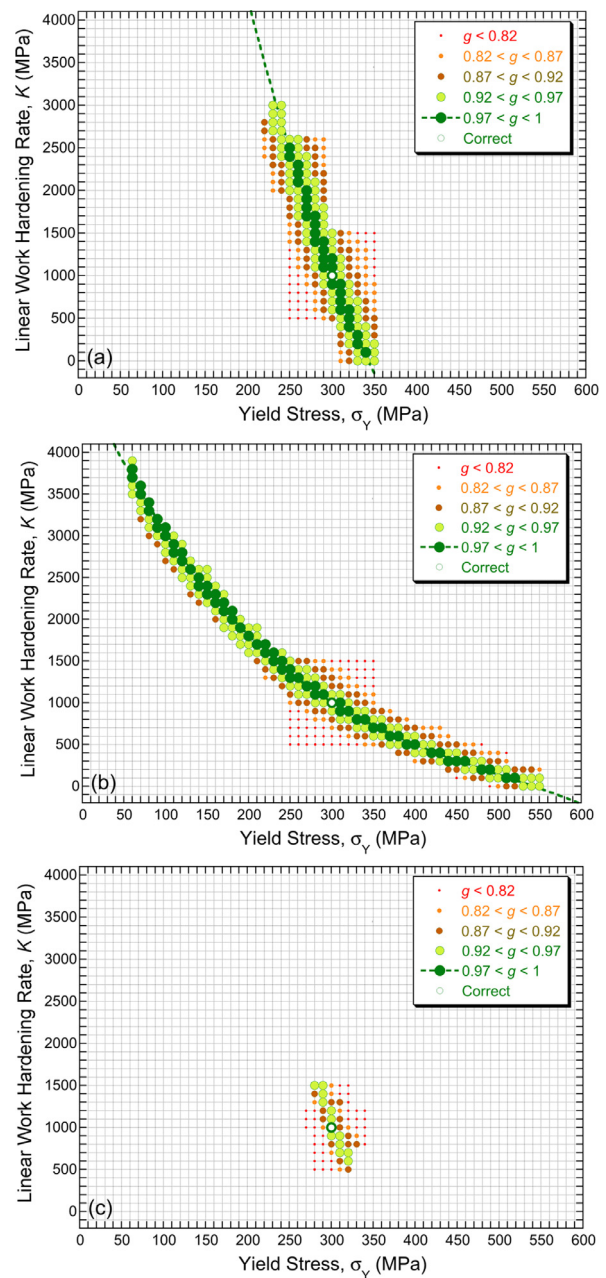


Fig. 8. Outcomes of FEM simulations for indentation into a linear work hardening material ($n=1$) with “correct” σ_Y and K values of 300 MPa and 1000 MPa, in the form of maps in σ_Y – K space, showing the ranges into which the g values fell for each simulation, for (a) sphere, (b) cone and (c) punch. The dotted lines are polynomial best fits for the points yielding g values above 0.97.

dotted lines. This is understandable, since, depending on the nature of the strain field (ie the indenter shape), the effect of having a σ_Y value below the “correct” one can be at least partly compensated by having a K value above the “correct” one (and vice versa). If only one such plot were available, there would be uncertainty about the validity of any inferred pair of values. However, an extra degree of freedom is injected by repeating the operation with a significantly different indenter shape. It can be seen in Fig. 8(b) that a similar “ridge” of high- g values appears for the cone, but it is inclined differently to the axes. These “ridges” intersect at the “correct” pair of values, which could therefore be obtained as the solution to the two polynomial expressions fitted to the sets of “high g ” points. This potentially constitutes a methodology for establishing

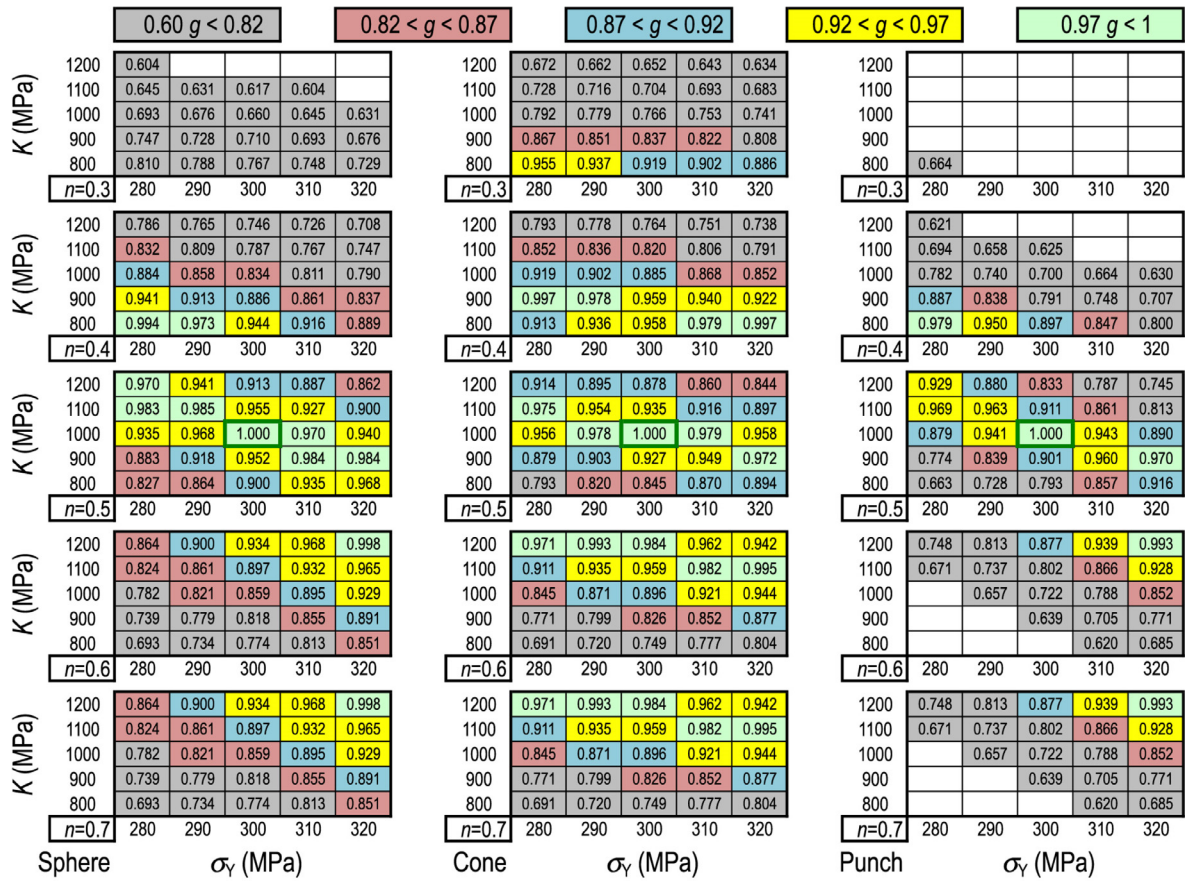


Fig. 9. Outcomes of FEM simulations, using spherical, conical and cylindrical (punch) indenters, for a material with “correct” yield stress, work hardening coefficient and work hardening exponent values of 300 MPa, 1000 MPa and 0.5. These are maps of g values in $\sigma_Y - K$ space, for five different values of n .

these values accurately, without the need for any complex convergence operations in parameter space.

However, simply taking the solution to be the intersection point between the lines representing the “high- g ridges” for two different shapes is unlikely to be reliable in all cases. This operation discards much of the g -data, including those defining the ends of the ridges. Moreover, while a second indenter shape will always tend to supply different information from the first, the gradients of the corresponding “ridges” could be similar, introducing large errors into the location of the “solution point”. This can be seen from the data for the punch, which produces a ridge with a similar gradient to that of the sphere, but a much shorter length, which is likely to be very helpful in obtaining the “best-fit” solution efficiently. In fact, this “ridge” is so short that only the “correct” parameter pair gives a value of g above 0.97. This is similar to the characteristics observed in Fig. 7(b) for the single parameter (σ_Y only) case. Of course, it’s important to appreciate that, when using real experimental data as the “reference” plot, noise will inevitably be introduced (partly because the actual stress-strain relationship may not conform closely to the assumed functional form) and the solution algorithm needs to be sufficiently robust to cope with this.

4.3. Power law work hardening

While some materials do exhibit approximately linear work hardening, at least over a certain strain range, it is often observed that the work hardening rate falls off at larger strains and a power law expression (Eq. (1)) is frequently used to represent the behavior over the complete strain range of interest (commonly up to about 20–30%, at least for ductile metals, although necking (or bar-

reling) often complicates the interpretation of experimental test data above about 10%). In this case, three parameter values are required, so a further degree of freedom is introduced into the problem, and it sounds plausible to expect three different indenter shapes to be needed in order to converge accurately on a solution. The three values chosen here for the reference (“correct”) case are $\sigma_Y = 300$ MPa, $K = 1000$ MPa and $n = 0.5$.

An analogous procedure to that in Section 4.2 has been followed, with the “ g -screening” operation now leading to a 3-D matrix of g values. The behavior follows similar trends to the 2-D case. Fig. 9 shows g maps in $\sigma_Y - K$ space, for five different values of n . The “ridges” of high g combinations are still observed, with the same tendency for these to be short with the punch. The “high- g ” combinations are now expected to lie in (curved) planes, rather than ridges. The nature of these planes is slightly more complex to interpret than in the case of the “high- g ” ridges in Fig. 8, but is nevertheless logical. It can be seen that a high value of n can compensate for having values of both σ_Y and K that are too high: this is because higher n values lead to the second term in Eq. (1) being smaller, at all strain levels below 100%. The behavior will change at strains above this level, but in practice it’s probably reasonable to take something like 30–40% as an extreme upper limit to the regime that should be explored (or is likely to be of any interest).

4.4. Solution algorithms using multiple indenter shapes

The observed characteristics give some clear pointers towards possible algorithms for identifying “best fit” combinations of parameter values. Equations for lines (2-parameter case) or planes

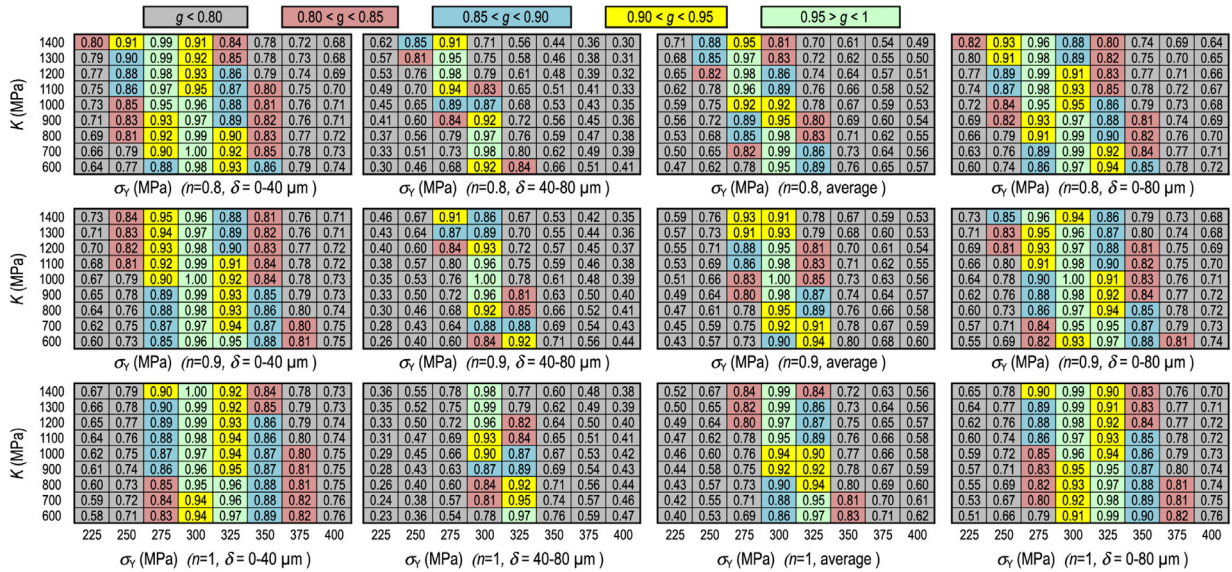


Fig. 10. Outcomes of FEM simulations of indentation with a 4 mm diameter sphere, using the displacement ranges shown, for a material with “correct” parameter values of $\sigma_Y = 300$ MPa, $K = 1000$ MPa and $n = 0.9$. These are maps of g values in $\sigma_Y - K$ space, for three different values of n .

(3-parameter case) could be formulated as best fits through a set of points in parameter space having g values above a specified cut-off level. The overall “best fit” parameter combination could then be the point of intersection of the two lines or the three planes. This suggests that the number of different indenter shapes will need to be the same as the number of parameters.

However, while there is some logic to this, it is almost certainly too simplistic and prone to error. A more robust procedure is likely to involve creating, for each indenter shape, a “cloud” in parameter space, comprising a set of (relatively high- g) points, each with its own g value. On superimposing multiple clouds (indenter shapes), a “master cloud” can be created (with each point having a g value given by the average for that point). The solution would then just be the point in the master cloud with the highest g value, although it’s likely to be helpful to also note the next few parameter combinations in the ranked list of g values.

On this basis, what needs to be specified in advance is: (i) the set of indenters to use, (ii) the functional form for the constitutive relation and (iii) the range of values for the parameters in that relation to be used for “ g -screening”. There is the issue of how fine that screening should be, and whether a second (finer) sweep should be carried out in the vicinity of the “coarse” solution, but these are computational details. Needless to say, the precision of the solution will be dependent on the reliability of the experimental load-displacement plots. There will, however, be scope for cross-checking of inferred parameter values, for example by comparing experimental and predicted residual indent shapes and by carrying out runs with further indenter shapes. Furthermore, the solution will always come with an associated g value, which can be used as some sort of indicator of the reliability of the outcome.

4.5. A single run, multi-partitioning approach

The above approach does not really require any particular number of indenter shapes, but it would appear that, unless there is only one unknown parameter (yield stress for a perfectly plastic material), it would be inadvisable to use only one shape. However, further consideration of this issue suggests that this is not necessarily true. **Provided the indenter shape is not self-similar**, then analysis of more than one section of a single load-displacement plot yields different sets of information, in an analogous way to

using different indenter shapes. This immediately points the way towards just using a single (spherical) indenter, and a single indentation run, with g -screening operations being carried out on more than one section of the load-displacement plot. This has obvious attractions, particularly since it allows the problems associated with all “sharp” indenters (Section 3.4) to be avoided.

The data presented in Fig. 10 suggest that this approach is viable. The figure shows the outcome of a g -screening operation on a single indentation run to a penetration depth of $100\mu\text{m}$, using a 4 mm diameter sphere, for a material with “correct” parameter values of $\sigma_Y = 300$ MPa, $K = 1000$ MPa and $n = 0.9$. These g values were obtained on sections of the load-displacement plot from the origin up to $40\mu\text{m}$ and from $40\mu\text{m}$ up to $80\mu\text{m}$. It can be seen that this operation, involving study of average g values for the two scans, allows effective convergence on the “correct” combination, in a similar way to the usage of different indenter shapes. The figure also shows the outcome (fourth column) of a single g -screening operation on the complete $0-80\mu\text{m}$ plot. It can be seen that the multiple scan operation does lead to sharper convergence (more efficient elimination of ambiguity) than a single operation on the same set of data. Of course, it’s important to recognize that real experimental data will incorporate noise that is absent from these purely FEM analyses, and also the possibility that the stress-strain relationship does not accurately fit the assumed functional form, so this is now investigated using the load-displacement data obtained for the copper.

5. Application to real experimental data (for copper)

The procedure described in Section 4.5 has been applied to the indentation data for the copper sample (Fig. 3). FEM runs were carried out, using a matrix of trial values of σ_Y , K and n . Of course, if this were an unknown material, then there might be little or no prior information available about probable values for these three parameters, so these runs covered a fairly broad range. The outcome is shown in Fig. 11. This g -screening operation was carried out on two sections of the $P(\delta)$ plot - for displacement ranges of $0-40\mu\text{m}$ and $40-80\mu\text{m}$. These ranges were chosen because: (i) they need to be significantly different in order to enhance the convergence efficiency, (ii) the early part of the plot (up to around $5\mu\text{m}$) is unlikely to be very reliable, because these displacements

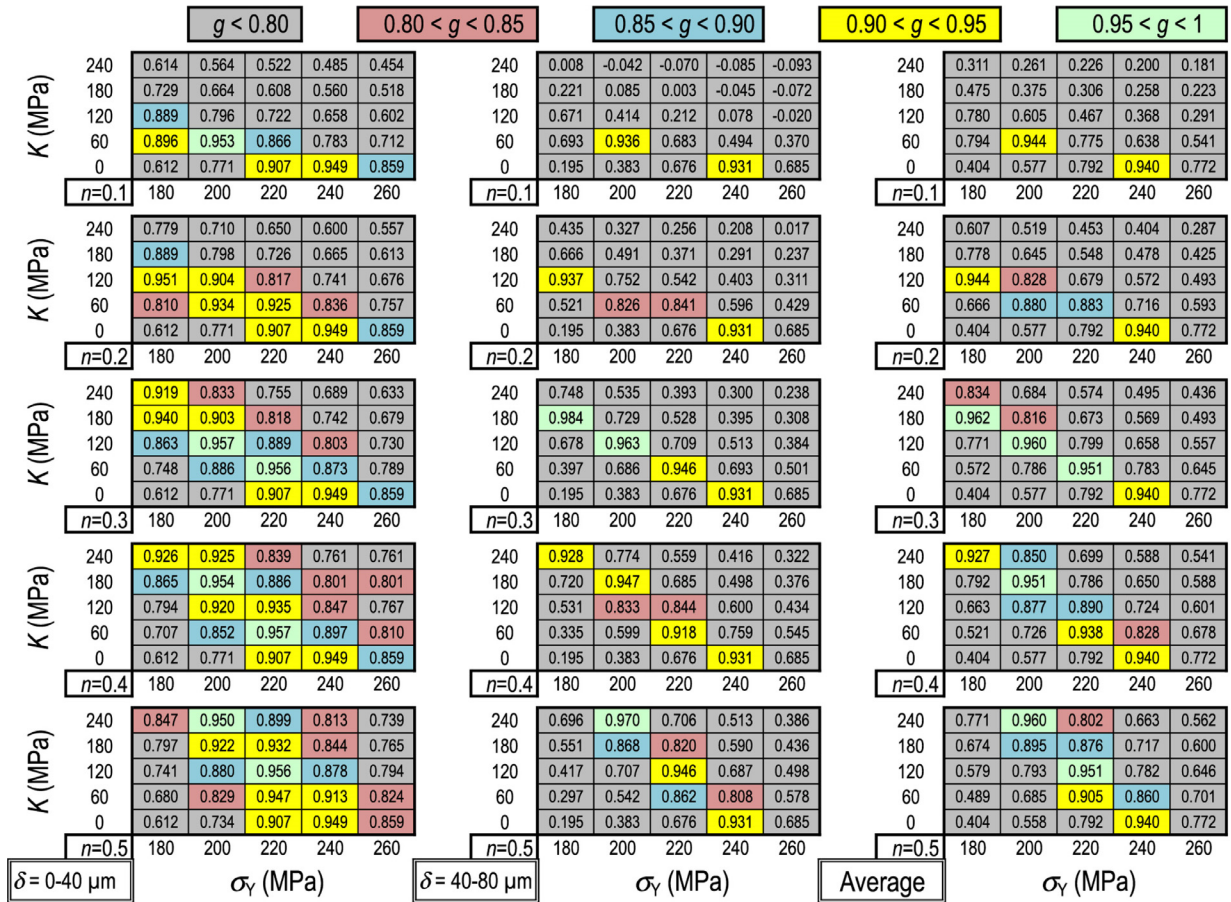


Fig. 11. Outcomes of FEM simulations, using the spherical indenter only and comparing predictions with experimental data over the two displacement ranges shown. These are maps of g values in $\sigma_Y - K$ space, for five different values of n .

are not much greater than the surface roughness and (iii) at large displacements ($> \sim 80 \mu\text{m}$), the strains in many regions are likely to be well beyond the range of interest, although the data in Fig. 7 illustrate that the strain range in which the $P(\delta)$ data are being strongly affected will be well below the peak values.

It can be seen in Fig. 11 that carrying out the g -screening on two different sections of the load-displacement plot does assist in the convergence, and at least partly removes the ambiguity that would result from a single scan. In this particular case, however, it does not lead to a single combination of parameter values that stands out as giving optimum agreement and no combination gives a g value very close to unity. This is unsurprising, since, as was mentioned in Section 2.2, the shape of the stress-strain curve does not, in this case, conform closely to any plot obtainable using Eq. (1). Nevertheless, the operation does lead to a good representation of the actual stress-strain relationship. It can be seen in Fig. 11 that there are several parameter combinations for which the average of the two comparisons yields a g value around the maximum (of about 0.960). For two of these ($\sigma_Y = 200 \text{ MPa}$, $K = 120 \text{ MPa}$, $n = 0.3$ and $\sigma_Y = 200 \text{ MPa}$, $K = 240 \text{ MPa}$, $n = 0.5$), Fig. 12 compares corresponding predictions with the experimental data for (a) the load-displacement plot and (b) the stress-strain curve. The latter shows that, while neither inferred plot conforms closely with the experimental one (and indeed no plot of Eq. (1) can do this), they are both giving fairly accurate descriptions. It is reasonable to suppose that, for a material with a stress-strain curve conforming closely to the assumed functional form, the (unique) solution, in the form of the three parameter values, could be accurately obtained using this methodology. Of course,

further detailed investigations are needed in order to confirm this.

6. Conclusions

The following conclusions can be drawn from this work:

- (a) The methodology of repeated FEM simulation of the indentation process, with systematic comparison between experimental and predicted outcomes, is basically sound and can in principle be used to infer a range of material properties. While the present work is focused on plasticity, the approach should be applicable to other properties, such as those related to creep. It will always be necessary to ascribe a functional form to the constitutive relations concerned, with the objective being to evaluate the parameters in these equations.
- (b) It is apparently necessary, at least in most cases, to carry out the indentation with more than one indenter shape, in order to remove the ambiguity that is likely to result from comparison between experiment and model for a single shape. However, it is clarified here that, provided the indenter shape is not self-similar, making multiple comparisons on different sections of the same load-displacement plot is similar in effect to the use of multiple indenter shapes. The viability of this procedure has been confirmed, leading to the attractive possibility of carrying out the experimental investigation in the form of a single indentation run with a sphere. A number of important advantages will result from

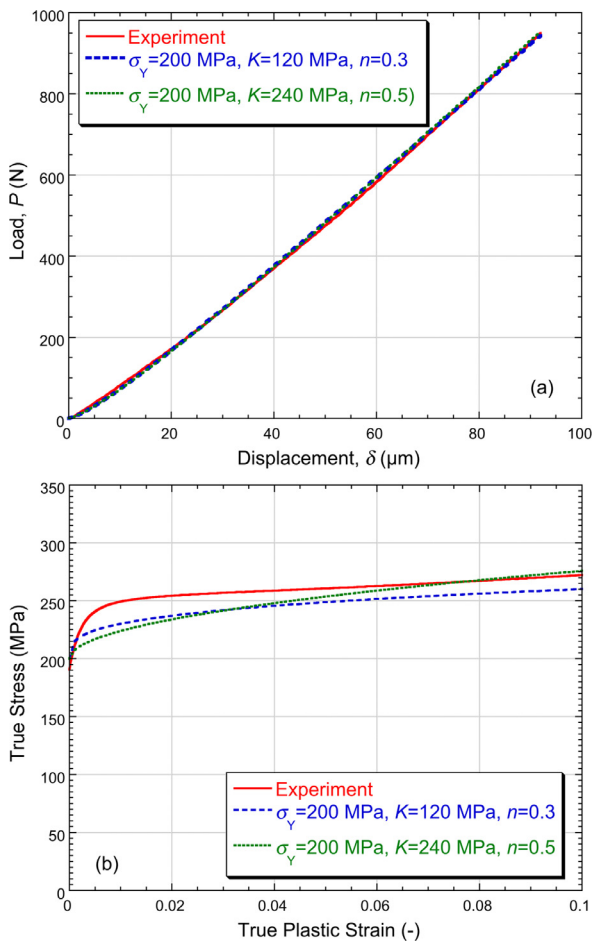


Fig. 12. Comparison between experimental data and predictions based on use of Eq. (1), with the two parameter sets shown (inferred via the g -screening operation), for (a) the indentation load-displacement plot and (b) the uniaxial stress-strain curve.

using a relatively large indenter diameter (probably with mm dimensions).

- (c) A methodology has been identified in which a goodness-of-fit parameter, g , is used to characterise the fidelity of model predictions, relative to experimental data. An operation of “ g -screening”, involving the creation of a cloud of g values in parameter space, is used to identify best-fit material property parameter combinations. The efficiency of this process, and confidence in the outcome, is likely to be increased by use of multiple indenter shapes or, as outlined above, use of multiple screening runs on different sections of a single load-displacement plot. The material used in the current investigation exhibits a stress-strain relationship that does not conform accurately to a simple functional form, and so could not be captured to very high precision using this methodology (or indeed any similar methodology). Nevertheless, this g -screening operation did lead to a representation of the plasticity characteristics that would be adequate for many purposes.
- (d) This work may serve to pave the way towards the development of user-friendly software packages, containing built-in resources for FEM implementation and g -screening operations, which would require the user only to specify the functional form of the constitutive relation and to input a single experimental indentation plot. In fact, there is already a website available (<http://www.simdent.com>) where a capability of this type is available.

Acknowledgements

This work has been supported by EPSRC (grant RG62695) and also by AWE, as part of an ongoing collaboration aimed at the development of robust and user-friendly tools for the extraction of mechanical property characteristics from instrumented indentation data.

In compliance with current EPSRC requirements, input data for the indentation modeling in this paper, including meshing and boundary condition specifications, are available at the following URL: www.ccg.msm.cam.ac.uk/publications/resources. These files can be downloaded and used in COMSOL FEM models. Data supplied are for a representative case (with a spherical indenter and radial symmetry).

References

- Alkorta, J., Martinez-Esnaola, J.M., Sevillano, J.G., 2005. Absence of one-to-one correspondence between elastoplastic properties and sharp-indentation load-penetration data. *J. Mater. Res.* 20, 432–437.
- Bobzin, K., Bagcivan, N., Theiss, S., Brugnara, R., Perne, J., 2013. Approach to determine stress strain curves by FEM supported nanoindentation. *Materialwissenschaft u. Werkstofftechnik* 44, 571–576.
- Bolzon, G., Maier, G., Panico, M., 2004. Material model calibration by indentation, imprint mapping and inverse analysis. *Int. J. Solids Struct.* 41, 2957–2975.
- Bouzakis, K., Michailidis, N., 2004. Coating elastic-plastic properties determined by means of nanoindentations and FEM-supported evaluation algorithms. *Thin Solid Films* 469, 227–232.
- Bouzakis, K., Michailidis, N., 2006. An accurate and fast approach for determining materials stress-strain curves by nanoindentation and its FEM-based Simulation. *Mater. Charact.* 56, 147–157.
- Bucaille, J.L., Stauss, S., Felder, E., Michler, J., 2003. Determination of plastic properties of metals by instrumented indentation using different sharp indenters. *Acta Materialia* 51, 1663–1678.
- Capehart, T.W., Cheng, Y.T., 2003. Determining constitutive models from conical indentation: sensitivity analysis. *J. Mater. Res.* 18, 827–832.
- Cheng, Y.-T., Cheng, C.-M., 2004. Scaling, dimensional analysis, and indentation measurements. *Mater. Sci. Eng.* 44, 91–149.
- Cheng, Y.T., Cheng, C.M., 1999. Can Stress-strain relationships be obtained from indentation curves using conical and pyramidal indenters. *J. Mater. Res.* 14, 3493–3496.
- Chollacoop, N., Dao, M., Suresh, S., 2003. Depth-sensing instrumented indentation with dual sharp indenters. *Acta Materialia* 51, 3713–3729.
- Dao, M., Chollacoop, N., Van Vliet, K.J., Venkatesh, T.A., Suresh, S., 2001. Computational modeling of the forward and reverse problems in instrumented sharp indentation. *Acta Materialia* 49, 3899–3918.
- Dean, J., Wheeler, J.M., Clyne, T.W., 2010. Use of quasi-static nanoindentation data to obtain stress-strain characteristics for metallic materials. *Acta Materialia* 58, 3613–3623.
- Fu, K.K., Chang, L., Zheng, B.L., Tang, Y.H., Wang, H.J., 2015. On the determination of representative stress-strain relation of metallic materials using instrumented indentation. *Mater. Des.* 65, 989–994.
- Futakawa, M., Wakui, T., Tanabe, Y., Ioka, I., 2001. Identification of the constitutive equation by the indentation technique using plural indenters with different apex angles. *J. Mater. Res.* 16, 2283–2292.
- Giannakopoulos, A.E., Suresh, S., 1999. Determination of elastoplastic properties by instrumented sharp indentation. *Scripta Materialia* 40, 1191–1198.
- Guelorget, B., Francois, M., Liu, C., Lu, J., 2007. Extracting the plastic properties of metal materials from microindentation tests: experimental comparison of recently published methods. *J. Mater. Res.* 22, 1512–1519.
- Hausild, P., Materna, A., Nohava, J., 2012. On the identification of stress-strain relation by instrumented indentation with spherical indenter. *Mater. Des.* 37, 373–378.
- Heinrich, C., Waas, A.M., Wineman, A.S., 2009. Determination of material properties using nanoindentation and multiple indenter tips. *Int. J. Solids Struct.* 46, 364–376.
- Herbert, E.G., Oliver, W.C., Pharr, G.M., 2006. On the measurement of yield strength by spherical indentation. *Philos. Mag.* 86 (33–35), 5521–5539.
- Herbert, E.G., Pharr, G.M., Oliver, W.C., Lucas, B.N., Hay, J.L., 2001. On the measurement of stress-strain curves by spherical indentation. *Thin Solid Films* 398, 331–335.
- Ma, Z.S., Zhou, Y.C., Long, S.G., Zhong, X.L., Lu, C., 2012. Characterization of stress-strain relationships of elastoplastic materials: an improved method with conical and pyramidal indenters. *Mech. Mater.* 54, 113–123.
- Patel, D.K., Kalidindi, S.R., 2016. Correlation of spherical nanoindentation stress-strain curves to simple compression stress-strain curves for elastic-plastic isotropic materials using finite element models. *Acta Materialia* 112, 295–302.
- Pelletier, H., 2006. Predictive model to estimate the stress-strain curves of bulk metals using nanoindentation. *Tribol. Int.* 39, 593–606.
- Xu, B.X., Chen, X., 2010. Determining engineering stress-strain curve directly from the load-depth curve of spherical indentation test. *J. Mater. Res.* 25, 2297–2307.